

# Design Optimization of a Covert Feather-Inspired Deployable Structure for Increased Lift

Chengfang Duan\* and Josiah Waite\*

University of Illinois at Urbana-Champaign, Urbana, IL, 61801, USA

Aimy A. Wissa<sup>†</sup>

University of Illinois at Urbana-Champaign, Urbana, IL, 61801, USA

### **Abstract**

Flying at low Reynolds numbers and at high angles of attack has always been a great challenge for unmanned aerial vehicles (UAVs). However, birds can easily perform these maneuvers in nature. Birds have passively-deployed feathers called covert feathers on the upper and lower surfaces of their wings. These feathers protrude into the flow to mitigate flow separation during high-angle-of-attack flight. This paper presents the design optimization of a single covert-inspired flap that is attached to the upper surface of an NACA 2414 airfoil. An evolutionary algorithim, known as The CMA-ES (Covariance Matrix Adaptation Evolution Strategy), is used for the design optimization. The objective function is to maximize lift and the design parameter is the flap deflection angle. The lift coefficient is calculated using an unsteady discrete vortex method (DVM). Preliminary results show that the optimal flap design improves lift up to 23% comparing with the clean airfoil at high angles of attack. This work is an important step towards achieving a spatially distributed deployable structures system, similar to the covert feathers, for separation control and stall mitigation in small unmanned air vehicles.

#### I. Introduction

Current mission demands for unmanned air vehicles (UAVs) require them to be adaptable, meaning the same flyer is required to perform multiple missions. In order to achieve this mission adaptability, UAVs are required to perform high angles of attack maneuvers, fly at slow and fast speeds, and through gusts of various magnitudes and profiles. During low-speed flight and high angle of attack maneuvers, flow reversal due to adverse pressure gradient frequently occurs. Flow reversal can lead to separation and eventually stall. Flow separation is undesirable because it reduces, and sometimes eliminates, the ability of a UAV to produce lift. Delaying stall and separation control are crucial during slow speed flight and high angle of attack maneuvers such as landing and perching. Moreover, delaying stall enables flight through gust where a sudden change of wind speed and direction can correspond to an abrupt increase in angle of attack.

In nature, birds are able to fly through adverse and harsh conditions by using their feathers, which can be viewed as spatially distributed deployable structures. These structures mitigate the adverse pressure effects, increase the maximum lift, and control separation. The wing feathers that are thought to be responsible for delaying stall are known as the covert feathers, shown in Figure 1. The covert feathers makeup almost as large a proportion of the total wing surface area as the other feathers combined. The coverts provide all of the upper surface contour and most of the lower surface contour over the thick forward sections of the airfoil.<sup>1</sup>

<sup>\*</sup>Graduate Research Assistant, Mechanical Science and Engineering Dept., 1206 W. Green Street, Urbana IL 61801, and AIAA Student Member.

<sup>&</sup>lt;sup>†</sup>Assistant Professor, Mechanical Science and Engineering Dept., 1206 W. Green Street, Urbana IL 61801, and AIAA Member.

The function of the covert feathers has been debated both in the engineering and biology communities. Some research efforts suggest that they operate similar to leading edge Kruger flaps, others claim that they act as vortex generators.<sup>3</sup> Recent studies based on free flight videos of a Steppe eagle show that the covert feathers are considered nature's equivalent of wing aero-elastic devices.<sup>4</sup> Moreover, studies show that the deployment of the covert feathers is dependent on the flight conditions and their location along the wing. For example, during high angle of attack maneuvers such as landing, take off, and perching, the lesser covert (sl) feathers on the lower side of the wing deploy. While during gust conditions, the upper wing greater covert (sg) feathers deploy. Figure 2 shows the covert feathers on the upper and lower

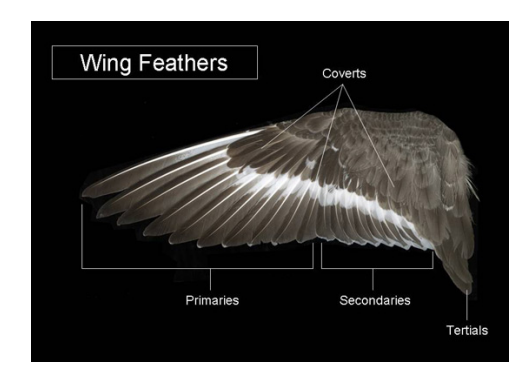


Figure 1: Major types of wing feathers showing the covert, primary, and secondary feathers.<sup>2</sup>

wing deployed during different flight maneuvers. The deployment of the covert feathers increases the maximum lift coefficient, which enables the birds to fly at slower speeds, in gust, and land in adverse weather conditions.

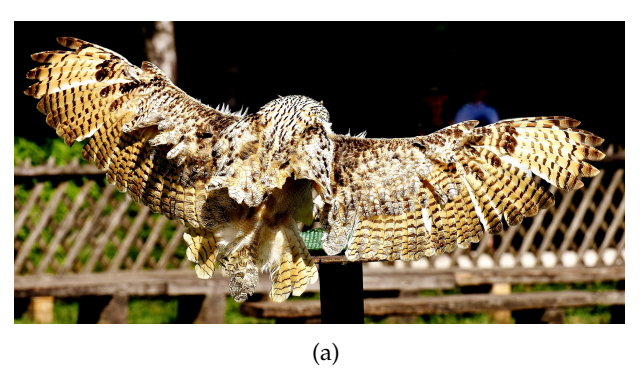




Figure 2: (a) An owl with its upper wing covert feathers deployed. (b) An owl during a perch with the lower wing covert feathers deployed.

There have been several studies, both numerical and experimental, that show either an increase of post-stall lift or a delay of stall due to covert-inspired flaps. <sup>5,6</sup> These studies are summarized in Section 2. Results from most of these studies show that covert-inspired flap is able to increase lift force, however, none of them provide a method to maximize the improvement by adjusting the flap design. Moreover, most of the studies published focus on modeling or measuring the aerodynamics but only a few investigate the effect of the geometric parameters and the spatial location of the deployable structures. In this paper, a design optimization methodology is studied to achieve the maximum lift for an NACA2414 airfoil by tailoring a single geometric parameter, namely the deflection angle, of a single covert-inspired flap mounted on the upper surface of an NACA2414 airfoil. This work is an important step towards achieving a spatially distributed deployable structures system (similar to the covert feathers) that can be used for separation control and stall mitigation in small unmanned air vehicles.

## II. Background

Meyer et al.<sup>5</sup> conducted a study that included both experimental and numerical analyses of a self-adjusting flap. They tested a single movable flap attached to a HQ17 wing in a wind tunnel, and developed a high-fidelity code that combined unsteady Reynolds-averaged Navier-Stokes simulations with large eddy simulations. Their tests and simulations were performed at a Reynolds numbers of about  $1 \times 10^6$ . They determined that the lift of the overall system could be enhanced by up to 10% by using a single flap on the suction side near the trailing edge of the wing. It was also determined that the main effect of the flap is blockage of reversed flow from the trailing edge to the leading edge. This led to a delay of flow separation.

The results of their analyses led them to conclude that the equilibrium position of a self-adjusting flap does not produce maximum lift, but that a lower flap deflection angle might. The authors suggest a torsion spring could be used to reduce the flap angle to achieve maximum lift for a particular configuration.

A similar study was conducted by Kernstine et al.<sup>7</sup> This study was conducted to analyze the effect of flap placement, flap size, and flap number on the overall lift. Wind tunnel tests at a Reynolds number of between  $1 \times 10^5$  and  $5 \times 10^5$  with a NACA 2412 airfoil showed that post-stall lift could be increased using a flap whose length was between 10% and 20% of the chord. Johnston and Gopalarathnam<sup>8</sup> drew different conclusions from a set of experiments run at a Reynolds number of  $4 \times 10^5$  that used a slightly different airfoil from Kernstine et al. These researchers used a 12%-thick cambered airfoil that was custom designed for conducting experiments in a specific wind tunnel. While the results from these tests did not show that the maximum lift coefficient for this airfoil increased, it did show that the angle of attack at which stall was experienced was increased with a flap present. This led to more gentle stall behavior.

Another study at a different Reynolds number of a self-adjusting flap was conducted by Schlüter. Water tunnel tests conducted by the authors at a Reynolds number of about  $4 \times 10^4$  also showed that post-stall lift is enhanced. Based on all the prior relevant work, post-stall lift enhancement due to the presence of a deployable flap was reported for a wide range of Reynolds numbers (from  $4 \times 10^4$  to  $1 \times 10^6$ ). This is important to note because the target for the current study is small UAVs which operate in that range. Schlüter was also involved in another study that investigated 3D effects of self-activated flaps on wings. Wang and Schlüter<sup>10</sup> performed a series of wind tunnel tests that studied the effects of flap span, flap chord length, and flap position along the wing's chord line. They concluded that placing a flap near the wing tip has little to no effect on the lift and that best performance is achieved when the flap span covers 80% of the wing span, leaving the 20% next to the wing tip clear. They also showed that changing flap chord and flap location along the wing's chord in their 3D model showed the same trends as those obtained with a 2D model.

Researchers have not only explored the passive nature of covert feathers (as with self-activated flaps in the studies previously mentioned), but they have also investigated active control techniques to mimic the functionality of covert feathers. Blower et al.<sup>11</sup> designed a wing structure with an array of panels that are actuator-controlled that mimic covert feathers. The authors implemented a feedback loop such that a panel's orientation is changed by an actuator in response to inbound gusts. Dhruv et al.<sup>12</sup> developed a low-order panel method with vortex particle wakes to analyze the aerodynamics of such a system.

The remainder of the paper is organized as follows. Section 3 presents the design optimization methodology, including the problem setup, optimization problem formulation, and the aerodynamic model. Section 4 discusses and validates the results from the design optimization. Conclusions and future work are presented in section 5.

## III. Design Optimization Methodology

#### A. Problem Set-up

The system analyzed in this paper is a two-dimensional airfoil with a single rigid flap mounted on the upper surface as shown in Figure 3. Important parameters include the airfoil angle of attack ( $\alpha$ ), the flap deflection angle ( $\beta$ ), the location of the root of the flap along the chord line of the airfoil ( $x_{flap}$ ), and the length of the flap ( $\ell_{flap}$ ). The values assigned to some of these parameters and used in the aerodynamic model are as follows:

Airfoil: NACA 2414
Reynolds Number = 200,000  $l_{flap} = 0.15c$   $x_{flap} = 0.8c$ 

The flap deflection angle ( $\beta$ ) is the design parameter for the optimization, therefore its value will be assigned by the design optimization algorithm to maximize the lift coefficient. The design optimization methodology is illustrated in Figure 4. The design optimization procedure is as follows:

• An initial estimate of the design variables is selected as the mean value of the initial generation,  $m^{(1)}$ . Set the initial step size,  $\sigma^{(1)}$ .

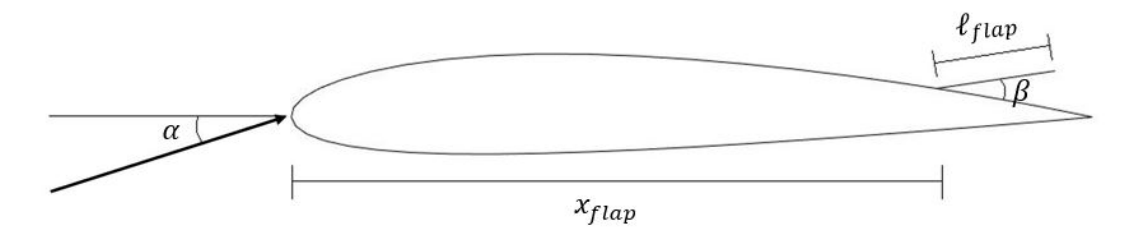


Figure 3: Definition of important geometrical parameters used in this study.

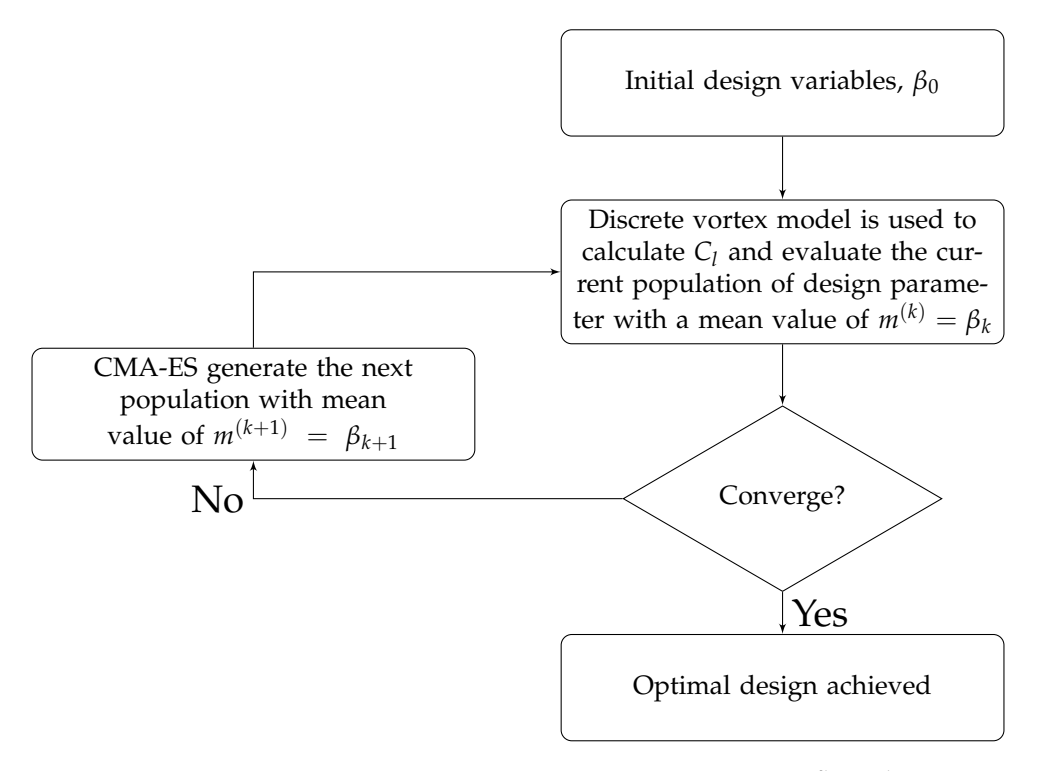


Figure 4: Design optimization flow chart

- A low-order unsteady discrete vortex method (DVM)<sup>13</sup> is used to calculate the lift coefficient to evaluate the current population. CMA-ES<sup>14</sup> is then used to generate the  $(k+1)^{th}$  generation, of which the mean value is  $m^{(k+1)}$ .
- The DVM model is called again, and the lift coefficient is then calculated for the new design points.
- The process is repeated until the mean value of the population converges at an optimal design point. Thus, the optimal flap deflection angle is determined at a given angle of attack.

#### **B.** Optimization Problem Formulation

CMA-ES was selected because it can account for the discontinuous derivatives of the objective function generated by DVM model. Moreover, CMA-ES can also accommodate a large number of design parameters. The number of design parameters will increase as more flaps are added to the airfoil's upper and lower surfaces and as three dimensional, instead of two dimensional, surfaces are considered. The design optimization can be expressed as:

$$\min_{\beta} -C_l(\beta) 
s.t. \quad \beta_{LB} \le \beta \le \beta_{UB}$$
(1)

where  $\beta_{LB}$  and  $\beta_{UB}$  are the lower and upper bounds for the flap deflection angle, respectively.  $\beta_{LB}$  was set to  $0^{\circ}$  and  $\beta_{UB}$  was set to  $30^{\circ}$ . The  $0^{\circ}$  deflection angle represents that the flap is not deployed. The upper bound for the flap deflection angle was determined based on experimental results from wind tunnel tests. The experimental setup and results are detailed in the article by Waite et al.<sup>15</sup>

#### C. Aerodynamic Model

At each optimization iteration, once a design population is generated, an unsteady discrete vortex methods model was used to calculate the lift coefficient for each given design. The vortex particle method is computationally efficient and is able to account for time dependency. Because it is a low-order method, calculation times are small, which makes it ideal for design purposes. It does, however, have some short-comings, including the requirement of a boundary layer model to account for viscous effects and the fact that it cannot directly compute pressure values. Despite its disadvantages, this method is best suited for the goals of this research by offering a fast way to evaluate multiple flap designs in the optimization loop given the unsteady and highly separated nature of the flow field. The DVM model is a low-order method that uses discrete vortices (also called vortons) to model an object's geometry and wake. These vortons induce a velocity in the flow. The velocity at a point of interest (x, z) induced by N vortices in the 2-D domain can be calculated using equation 2. u and w are the induced velocity components in x and z directions, respectively,  $r_i$  is the position vector from the  $i^{th}$  vortex to a point of interest,  $\Gamma_i$  is the  $i^{th}$  vortex circulation, and z is a reduction factor. The reduction factor prevents the induced velocity from going to infinity when z gets close to zero, making the DVM model more robust.

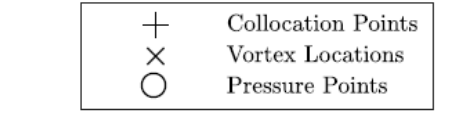
$$[u,w] = \frac{1}{2\pi} \sum_{i}^{N} \Gamma_{i} g^{\frac{[z-z_{i},-(x-x_{i})]}{|r_{i}|^{2}}}$$
(2)

At separation points along the geometry, some vortons are shed into the wake. The shed vortons are tracked over time, making this method an unsteady analysis. In the current work, in order to model the effects of flow separation, wake vortices are shed from not only the trailing edge but also along the upper surface of the airfoil. Separation locations at different angles of attack were determined *a priori* using XFOIL.<sup>16</sup>

Due to the no penetration boundary condition through the airfoil surfaces, the velocity induced by the body and wake vortices at collocation points (Fig. 5) should be equal to the normal velocity. Thus, the circulation of body vortices can be calculated by

$$[I]_{body}\{\Gamma\}_{body} + [I]_{wake}\{\omega\}_{wake} = \{v\}_{\perp}$$
(3)

where I is the influence matrix,  $\{\Gamma\}_{body}$  is the circulation of the body vortices,  $\{\omega\}_{wake}$  is is the circulation of the wake vortices, and  $\{v\}_{\perp}$  is the normal component of the velocity at collocation points.



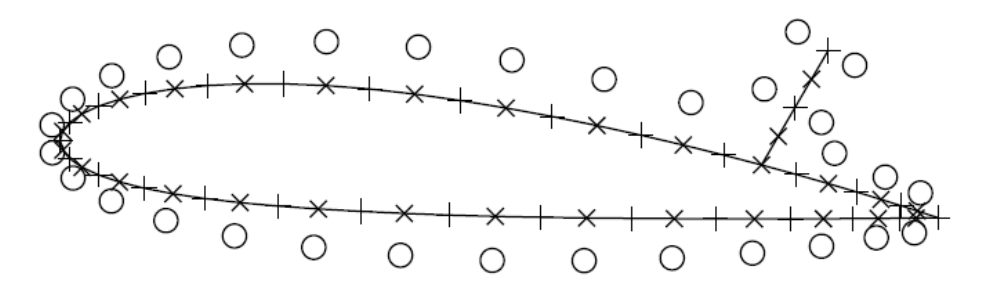


Figure 5: Visualization of the DVM's geometry.

Once the circulation of the airfoil body and wake vortices are computed, pressure points were selected around the airfoil based on a boundary layer model, as shown in Figure 5. In order to predict pressure in separated flows, Uhlman's formulation was applied to calculate the pressure and lift values at pressure points. Formulation and details of Uhlman's method can be found in.<sup>17</sup>

#### IV. Results and Discussion

The lift coefficient of a NACA 2414 airfoil is calculated using the DVM mode for validation and to serve as a baseline. As shown in Figure 6, the DVM provide comparable lift coefficient values with existing experimental data conducted by Selig et al. Figures 7 illustrate the search path of the optimal design for a flap located at 0.8c at different angles of attack.  $x_{mean}$  is the mean value of each design population, which represents  $\beta$ , and  $f(x_{mean})$  is the objective function value evaluated at  $x_{mean}$ , which represents  $-C_l$ . The initial flap deflection angle was set to be  $20^\circ$  for all cases. Figures 7d, 7b, 7a show that an optimal flap design is reached when  $\beta=12^\circ$  for  $\alpha=13^\circ$ ,  $15^\circ$ , and  $16^\circ$ , respectively. Figure 7c shows that at  $\alpha=14^\circ$ , an optimal design is found at  $\beta=5^\circ$ . Figure 7e shows that at  $\alpha=10^\circ$ , an optimal design is found after at  $\beta=0^\circ$ .

Table 1 summarizes the lift coefficient produced by DVM for the NACA 2414 airfoil without a flap and with the optimal flap design at different angles of attack. The optimal flap deflection angle at  $\alpha = 10^{\circ}$  is  $0^{\circ}$ . This is because, at  $\alpha = 10^{\circ}$ , flow above the upper surface of the airfoil is still attached leading to an adverse effect on lift production when the flap is deployed. Conversely, at higher angles of attack, when the flow is not fully attached, the deployment of the flap has a favorable effect on lift. At these angles of attack, a flap deflection angle of 12° almost always provides the large improvement in lift coefficient, even though it is a sub-optimal solution at  $\alpha = 14^{\circ}$ . The optimal flap deflection angle and the percentage improvement in lift coefficient both show good agreement with the wind tunnel experiment, as shown in Figure 8. From the wind tunnel experiment results, the flap deflection angle to provide the most improvement in lift coefficient is between 10° and 15°. Details of the wind tunnel experiment can be found in Waite et al. 15 Thus, the DVM-based design optimiza-

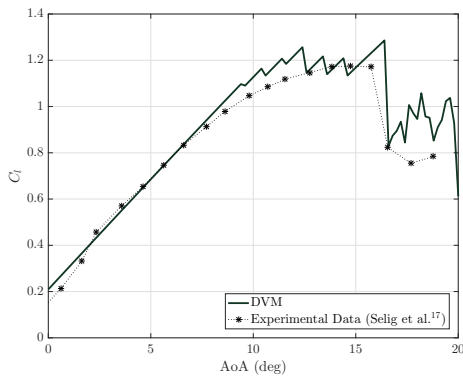


Figure 6: Lift coefficient versus angle of attack for the NACA 2414 airfoil without a flap. The lift values calculated using the DVM model agrees with archival experimental data.<sup>18</sup>

tion proved to be sufficient in producing optimal solutions that show agreement with experimental results while remaining computationally efficient.

RANS-based computational fluid dynamic (CFD) simulations were conducted using COMSOL Multiphysics. These simulations were used to determine the effect of the flap on the flow field and pressure coefficient. An airfoil at angles of attack of  $16^{\circ}$ ,  $13^{\circ}$ , and  $10^{\circ}$  were tested without a flap and the same simulations were repeated with a flap deployed at  $12^{\circ}$ . The SST turbulence model was used to close the RANS equations. Table 2 shows the velocity magnitude and pressure coefficient ( $C_p$ ) comparison between the baseline airfoil (the airfoil without a flap) and the airfoil with a flap deployed at  $12^{\circ}$ . The airfoil was set to angles of attack of  $16^{\circ}$ ,  $13^{\circ}$ , and  $10^{\circ}$ . The velocity magnitude plots show that at angles of attack of  $16^{\circ}$  and  $13^{\circ}$ , an airfoil with a flap has significantly smaller wake region. While at an angle of attack of  $10^{\circ}$ , the effect of the flap on the wake region is negligible. The  $C_p$  comparison at an angle of attack of  $16^{\circ}$  and  $13^{\circ}$  show a pressure recovery step at the flap root location. Moreover, an airfoil with a flap deployed at the optimal deflection angle results in a higher suction peak when compared to the baseline airfoil. Similar results were found in an experimental study in the literature, where the flap was described as a "pressure dam" allowing lower pressures upstream of the flap location.

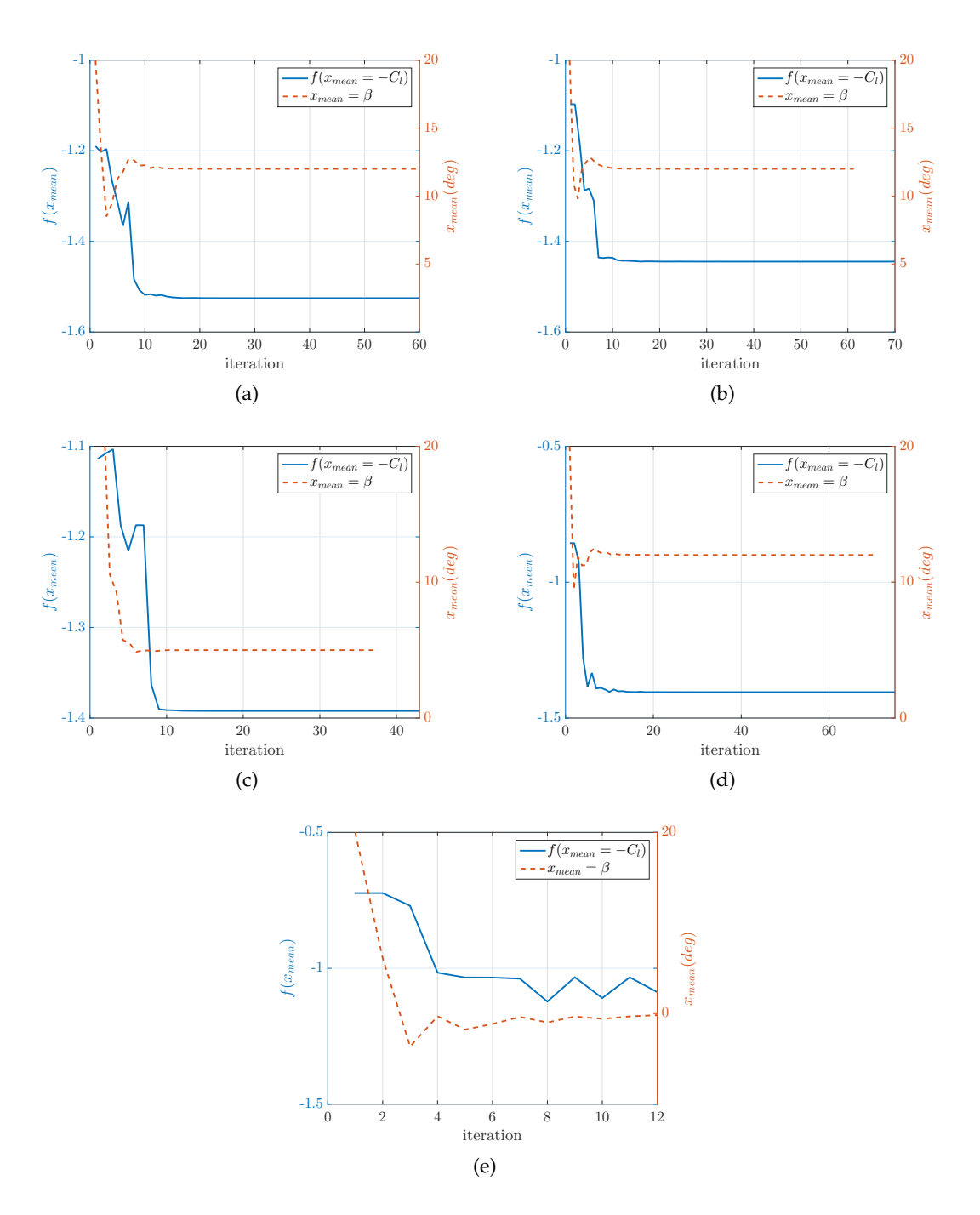


Figure 7: The design optimization search path at (a)  $\alpha = 16^{\circ}$ , (b)  $\alpha = 15^{\circ}$ , (c)  $\alpha = 14^{\circ}$ , (d)  $\alpha = 13^{\circ}$ , and (e)  $\alpha = 10^{\circ}$ .  $x_{mean}$  is the mean value of each design population, which represents  $\beta$  (the flap deflection angle).  $f(x_{mean})$  is the objective function value evaluated at  $x_{mean}$ , which represents  $-C_l$ .

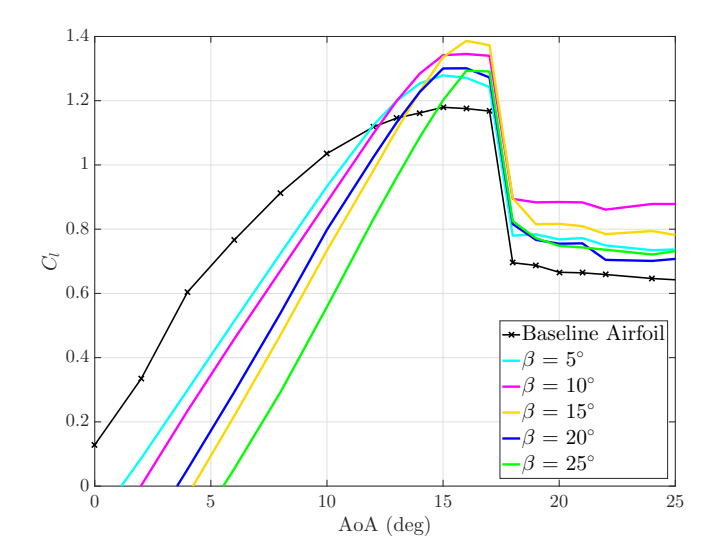


Figure 8: Experimental lift coefficient versus angle of attack for a flap located at  $x_{flap} = 0.8c$  at different flap deflection angles. The lift values for the airfoil without a flap is compared to archival experimental data. <sup>18</sup>

Table 1: Improvement of Lift coefficient at different angle of attack (	$\alpha$	)

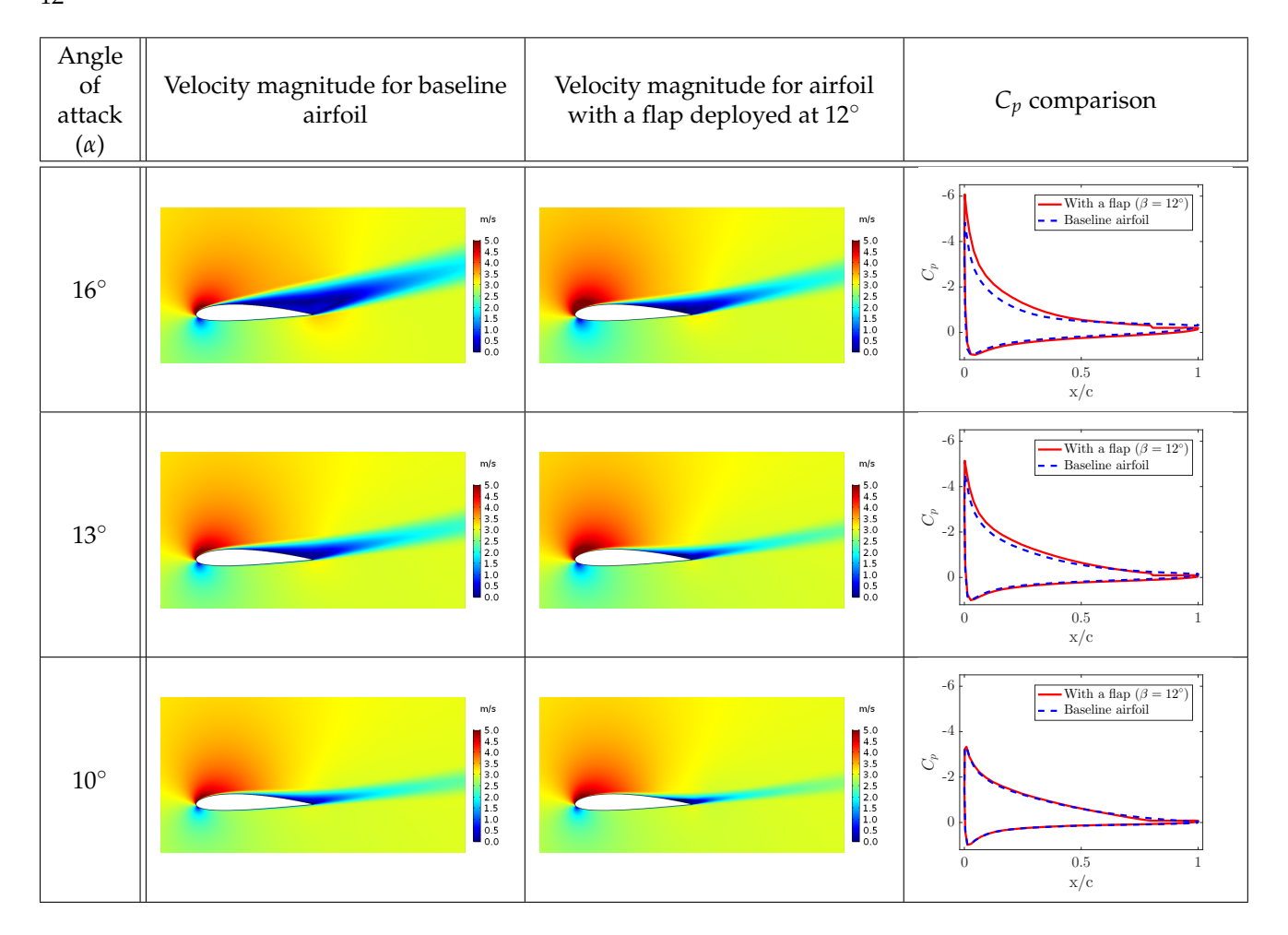
Angle of attack (α)	Optimal flap deflection angle $(\beta)$	Lift coefficient for airfoil without a flap	Lift coefficient for airfoil with optimal flap design	improvement of Lift coefficient
16°	12°	1.25	1.53	22.4%
15°	12°	1.17	1.44	23.1%
14°	5°/12°	1.17	1.40/1.38	19.7%/18.0%
13°	12°	1.18	1.40	18.6%
10°	0°	1.13	1.13	0%

## V. Conclusions and Future Work

This paper presented the design optimization methodology for a covert-inspired deployable flap. The flap was mounted to the upper surface of a NACA 2414 airfoil. The optimization algorithm is an evolutionary algorithm, where the airfoil lift coefficient was used as the objective function and the flap deflection angle was used as the design variable. The lift coefficient was computed using an unsteady discrete vortex method. Optimization results show that an optimal flap design can be reached and lift improvements up to 23% can be achieved at high angles of attack, which agrees with experimental results.

The discrete vortex method showed an advantage in computational efficiency, making it a suitable tool for design purposes. Future work includes modifying the DVM model such as expanding the applicability of the model to a wider range of angles of attack and including other design parameters such as the flap's location along the chord and length. Future work also includes modeling and optimizing multiple flaps in the chord and span directions, as well as designing, modeling, and testing a flap deployment mechanism that is can passively induce the optimal flap deflection angle under a given aerodynamic load.

Table 2: Velocity magnitude and  $C_p$  comparison between baseline airfoil and airfoil with a flap deployed at  $12^{\circ}$ 



#### References

<sup>1</sup>Graham K. Taylor, Anna C. Carruthers, Tatjana Y. Hubel, and Simon M. Walker. Wing Morphing in Insects, Birds and Bats: Mechanism and Function, 2012.

<sup>2</sup>U.S. Fish and Wildlife Service. Feather atlas. https://www.fws.gov/lab/featheratlas/.

<sup>3</sup>John J. Videler. Avian Flight. 2005.

<sup>4</sup>Anna C. Carruthers, Adrian L.R. Thomas, and Graham K. Taylor. Automatic aeroelastic devices in the wings of a steppe eagle Aquila Nipalensis. *The Journal of Experimental Biology*, 210(Pt 23):4136–4149, 2007.

<sup>5</sup>Robert Meyer, Wolfram Hage, Dietrich W. Bechert, Markus Schatz, Thilo Knacke, and Frank Thiele. Separation control by self-activated movable flaps. *AIAA journal*, 45(1):191–199, 2007.

 $^6$ G-ograve, tz Bramesfeld, and Mark D Maughmer. Experimental Investigation of Self-Actuating, Upper-Surface, High-Lift-Enhancing Effectors. *Journal of Aircraft*, 39(1):120–124, jan 2002.

<sup>7</sup>Kemp H. Kernstine, Courtney J. Moore, Andrew Cutler, and Rajat Mittal. Initial characterization of self-activated movable flaps, "pop-up feathers". *AIAA paper*, 369, 2008.

<sup>8</sup>Joe Johnston and Ashok Gopalarathnam. Investigation of a bio-inspired lift-enhancing effector on a 2d airfoil. *Bioinspiration & biomimetics*, 7(3):036003, 2012.

<sup>9</sup>Jörg Schlüter. Lift enhancement at low reynolds numbers using self-activated movable flaps. *Journal of Aircraft*, 47(1):348–351, 2010.

<sup>10</sup>C.H. John Wang and Jörg Schlüter. Stall control with feathers: Self-activated flaps on finite wings at low reynolds numbers. *Comptes Rendus Mécanique*, 340(1):57–66, 2012.

<sup>11</sup>Christopher J. Blower, Woody Lee, and Adam M. Wickenheiser. The development of a closed-loop flight controller with panel method integration for gust alleviation using biomimetic feathers on aircraft wings. In *Proc. of SPIE Vol.*, volume 8339, page 83390I.

<sup>12</sup>Akash Dhruv, Christopher Blower, and Adam M. Wickenheiser. A three dimensional unsteady iterative panel method with vortex particle wakes and boundary layer model for bio-inspired multi-body wings. In *SPIE Smart Structures and Materials+ Nondestructive Evaluation and Health Monitoring*, page 94290M. International Society for Optics and Photonics, 2015.

- <sup>13</sup>Josiah Waite, Chengfang Duan, Greg Reich, and Aimy Wissa. Aeroelastic Model for the Design of Covert-Inspired Passively-Deployable Structures. In 27th International Conference on Adaptive Structures and Technologies, pages 1–16, Lake George, NY, 2016.
  - <sup>14</sup>Nikolaus Hansen. The cma evolution strategy: A tutorial. arXiv preprint arXiv:1604.00772, 2016.
- <sup>15</sup>Josiah Waite, Chengfang Duan, Mihary Ito, Aimy Wissa, Hazem S. Eldahshan, Mohamed Khairy, and Mohamed H. Elalfy. Design methods for covert-inspired passively-deployable lift-enhancing structures. *Journal of Aircraft, in preparation*, 2017.
- <sup>16</sup>Mark Drela. Xfoil: An analysis and design system for low reynolds number airfoils. In *Low Reynolds number aerodynamics*, pages 1–12. Springer, 1989.
- <sup>17</sup>J.S. Uhlman Jr. An integral equation formulation of the equations of motion of an incompressible fluid. Technical report, DTIC Document, 1992.
- <sup>18</sup>Michael S. Selig, Phillipe Giguère, Cameron P. Ninham, and James J. Guglielmo. Summary of low speed airfoil data, volume 2. SoarTech, 1996.
- <sup>19</sup>G-ograve, tz Bramesfeld, and Mark D Maughmer. Experimental investigation of self-actuating, upper-surface, high-lift-enhancing effectors. *Journal of aircraft*, 39(1):120–124, 2002.